Nanosized Nickel(or Cobalt)/Graphite Composites for Hydrogen Storage

Z. Y. Zhong, Z. T. Xiong, L. F. Sun, J. Z. Luo, P. Chen, X. Wu, J. Lin,* and K. L. Tan

Department of Physics, Surface Science Laboratory, National University of Singapore, 10 Kent Ridge Crescent, Singapore 117542

Received: January 17, 2002; In Final Form: July 6, 2002

To seek new potential materials for hydrogen storage, an arc-discharge method was employed to prepare nanosized nickel(or cobalt)/graphite composites, in which the nickel (or cobalt) particles were highly dispersed in a carbon matrix with particle size between 20 and 70 nm (or 5−20 nm). Quantitative TPD measurements showed that at about 500 °C and 30−50 atm these nanosized composites could uptake up to 2.8 wt % H_2, which can be released at 500 °C and 1 atm. The addition of Ni (or Co) in C was found to largely enhance the H_2 adsorption, with the optimal amount of Ni being 20 wt %. In-situ FTIR showed that hydrogen was dissociatively adsorbed only in the presence of a transition metal and bonded to carbon atoms forming C−H bond. The hydrogen adsorption/desorption could be recycled. However, the capacity decreased to 1.6 wt % after 5 cycles. TEM, XPS, and BET surface-area and pore-volume measurements revealed that some of the transition metal particles migrated out from the carbon matrix and agglomerated after the H_2 adsorption/desorption cycles, which may reduce the transition metal−carbon synergism and thus the H_2 storage capacity. Under low temperatures below −120 °C and moderate pressures above 6 atm hydrogen storage by these Ni(or Co)/C composites could be detected. Storage capacity up to 2.7 wt % for Ni/C was measured by PCI at 77 K and 70 atm.

Introduction

Hydrogen is an ideal energy carrier. Using hydrogen as a fuel is an environmental friendly approach that produces almost zero pollution emissions. In the last several decades efficient hydrogen storage and transportation have been the major concerns and issues in the energy technology. One of the systems for hydrogen storage that has been extensively studied is the metal and alloy hydrides,[1−5] in which hydrogen is located in the form of atoms on interstitial sites of the host metal lattice. In recent years there have been hectic research activities on the hydrogen-storage technology based on carbon nanotubes (CNTs).[6−11] But most of these researchers studied CNTs without metal doping, and there are still disputes about the capacities of hydrogen storage in carbon nanotubes.[10,12]

Doping of alkaline metals in carbon nanotubes was attempted in 1999 and was claimed to have greatly enhanced the H_2 storage capacity at ambient pressure and moderate temperature range.[13] It was later proved that in this experiment weight increase as measured by thermogravimetric analysis was due largely to moisture rather than H_2 uptake.[14,15] Nevertheless metal-assisted hydrogen uptake by carbon materials was reported to be feasible in several patents and papers, in which a minor amount of a transition metal such as Pd or Pt dispersed in carbon could dissociate hydrogen molecules into hydrogen atoms, which could then spill onto nearby available storage sites on the carbon, hence increasing the hydrogen storage capacity of the carbon.[16,17] In some cases, the combination of metals with carbon in composites was found to create new sites for hydrogen adsorption.[18]

In this paper, an arc-discharge method was employed to prepare nanosized Ni(or Co)/graphite composites. Their hydrogen uptake/release behavior was studied by quantitative temperature-programmed desorption (TPD), as well as by pressure−composition isotherm (PCI). TEM, Raman scattering, XRD, and BET surface area, and pore volume measurements were employed to study their nanostructures before and after hydrogen adsorption and desorption cycles. The role of transition metals in the hydrogen uptake by carbon was discussed.

Experimental Section

The direct current arc-discharge experiments were performed in a home-built stainless steel chamber in helium gas under a pressure of 500 Torr. A voltage of 70−80 V was applied to the two graphite electrodes (Aldrich). The diameter of the anode and cathode is 6 mm and 14 mm, respectively. Prior to the arc-discharge process, a hole with a diameter ca. 4 mm was drilled in the anode rod to fill in catalysts. The catalyst consisted of graphite and nickel (or cobalt) powders (Aldrich). Various Ni/graphite ratios were adopted for comparative studies. During the arc-discharge process, the electric current was controlled at around 75A. The arc-discharge deposit on the wall of the chamber was collected for further measurements.

Hydrogen-storage measurements were carried out using a home-built stainless steel microreactor equipped with an on-line gas chromatography (GC 8000, Thermoquest Italia) and an on-line mass spectrometer (HPR20 mass spectrometer, Hiden Analytical Ltd). The sample (ca. 300 mg) positioned in the middle of the microreactor was heated to 700 °C in a flow of purified argon and held at 700 °C till GC baseline became smooth. The feed gas was changed to hydrogen gas for hydrogen adsorption after the sample had been cooled to room temperature in argon. Typically the absorption of hydrogen gas was conducted from room temperature up to 500 °C under a hydrogen pressure of 35 atm. Previously we had proved that there was no catalytic reaction below 500 °C between the hydrogen and the carbon under our experimental conditions.

* Corresponding author. Fax: +65-777-6126. E-mail: phylinjy@nus.edu.sg.

10.1021/jp020151j CCC: $22.00
Published on Web 08/24/2002

After cooling to room temperature in hydrogen, the sample was purged with argon gas again and successively a programmed temperature desorption (TPD) was performed from room temperature up to 700 °C at a heating rate of 10 °C/min, using argon as carrier gas. The amount of hydrogen desorbed from the H_2-saturated samples was analyzed quantitatively by the on-line GC and MS and calibrated by comparing their integrated area of TPD peaks with that of the hydrogen gas of a defined volume. The results from the TPD method were quantitatively in good agreement with those measured by a volumetric measurement using a pressure composition isotherm (PCI) manufactured by the Advanced Materials Corporation of Pittsburgh, PA. In volumetric measurement the effect of trace moisture in the feed gas could be eliminated. The consistency between TPD and PCI data ensured the reliability of the measurements.

The hydrogen adsorption and desorption of the samples at low temperatures were studied on an Intelligent Gravimetric Analyzer (IGA-003, HIDEN Analytical Ltd) which could monitor the sample weight change due to the gas adsorption/desorption in wide ranges of temperature (liquid nitrogen temperature to 800 °C) and pressure (10^{-6} Torr to 10 atm). The sample was first outgassed in a vacuum, heated to 700 °C, and then cooled to room temperature. Sequentially, the hydrogen gas was introduced to the sample chamber. The temperature was further cooled to liquid nitrogen temperature while the weight increase of the sample, corresponding to physically adsorbed hydrogen, was recorded.

The metal content in the prepared nanocomposites was analyzed by thermal gravimetric analysis (TGA, Mettler Toledo). For each measurement, approximately 30 mg of the sample was burned out in a flow of 10 vol % O_2 in Ar gas in a temperature-programmed oxidation mode (TPO). To ensure full burning out of the carbon, a low heating rate (3 °C/min) and a high TPO upper temperature of 1000 °C were selected. The residual after the burning was the metal in the form of its oxide. After the deduction of the oxygen weight, the metal content could be obtained.

XPS study was conducted on a VG ESCALAB-MKII spectrometer using Al Kα X-ray source at the constant analyzer pass energy of 20 eV. All binding energies (BE) were referenced to the C 1s core-level peak at 285.4 eV obtained with the sample powder.

The nanostructure and the morphology of all samples were observed employing a JEM-100CX transmission electron microscope (TEM) with a high voltage of 100 kV. X-ray powder diffraction (XRD) was performed on a Bruker D8 Advance diffractometer with a Cu target and a scanning step of 0.05°/s. The Raman scattering spectra were obtained with a Renishaw System 2000 at room temperature with a laser beam of 514 nm. The typical laser power was 1 mW and the acquisition time for each spectrum was 10 s. A 50× objective was employed, giving an illuminated spot of about 2 μm in diameter. The spectral resolution was 1 cm^{-1}. Specific surface area and pore distribution property measurements were conducted on a Nova 3000 instrument (Quantachrome Corporation) by BET method at liquid-nitrogen temperature. FTIR spectra were recorded on a Perkin-Elmer System 2000.

Results and Discussion

1. Characterization of Ni(Co)/C Composites by TEM, X-ray Diffraction, and Raman Backscattering. The Ni(Co)/C samples after the arc-discharge process were investigated by TEM. Figure 1a is a TEM image of a mixture of nickel and graphite before arc-discharge, in which the graphite-layered structure is clearly discernible. In this mechanical nickel and graphite mixture the size of the metallic nickel particles mostly ranged from 0.3 to 1 μm, and the graphite particles from 1 to 5 μm. Figure 1b is the image for an arc-discharged Ni/C composite, Ni_{20}(arc). The arc-discharge-derived products are denoted with the composition of their catalysts. For example Ni_{20}(arc) is the deposit on the wall of the chamber, derived from the arc-discharge of the Ni(20 wt %) and graphite(80 wt %) mixture. In this sample, nickel particles are highly dispersed in the carbon matrix, with particle size from 20 to 70 nm, and very few single-walled carbon nanotubes could be observed. For Co-containing graphite samples after the arc-discharge process, cobalt particles are dispersed even better, mostly in the range of 5−20 nm (see Figure 1c for Co_{40}(arc)). Some single-walled carbon tubes were observed, but their content was estimated to be less than 3%. Without the metal addition in the anode catalyst, pure graphite also underwent a dramatic change in particle size after arc-discharge (Figure 1d). It is obvious that arc-discharge processing results in the dramatic decrease in particle size as well as the high dispersion of metals in carbon. This is easily understood since the temperature is rather high in the arc spots in which most of components are vaporized or melted. The component molecules in the vapor state were condensed quickly through escaping from the arc spots and depositing on the chamber wall and cathode to form small particles, even small clusters and carbon tubes. Samples collected from different places of the arc-discharge chamber may show different structures. In the cathode deposits, besides the multiwalled carbon tubes, amorphous carbon, and polyhedral graphite particles, large nickel particles could be observed (above 100 nm, Figure 1e).

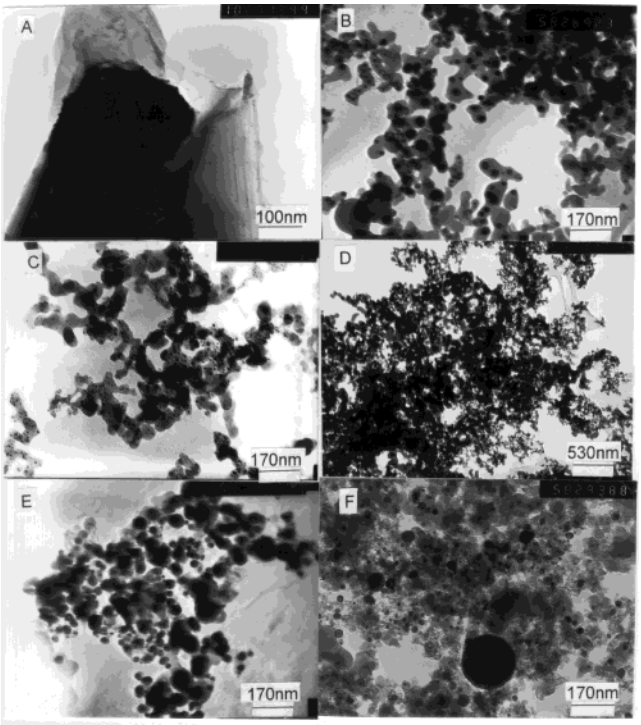

Figure 1. Typical TEM micrographs of (a) the mixture of graphite with nickel before arc-discharge; (b) Ni_{20}(arc), the deposit on the wall of the arc-discharge chamber using a catalyst containing 20 wt % Ni and 80 wt % graphite; (c) Co_{40}(arc); (d) C(arc), pure graphite after arc-discharge; (e) deposit on cathode for Ni_{20}(arc) sample; (f) the Ni_{20}-(arc) sample after 5 cycles for hydrogen adsorption and desorption.

The samples produced by the arc-discharge process were further investigated by XRD and Raman backscattering. Figure

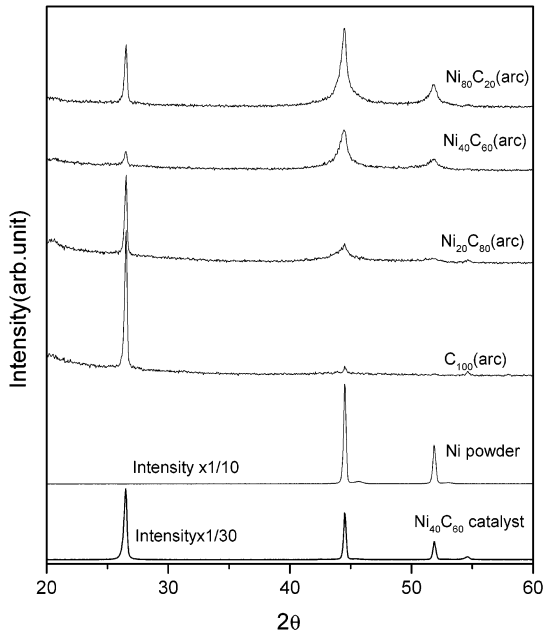

Figure 2. XRD patterns of the Ni-containing catalyst mixtures and their arc-discharge deposits (marked with arc) on the wall of the arc-discharge chamber. The weight composition of each catalyst is marked.

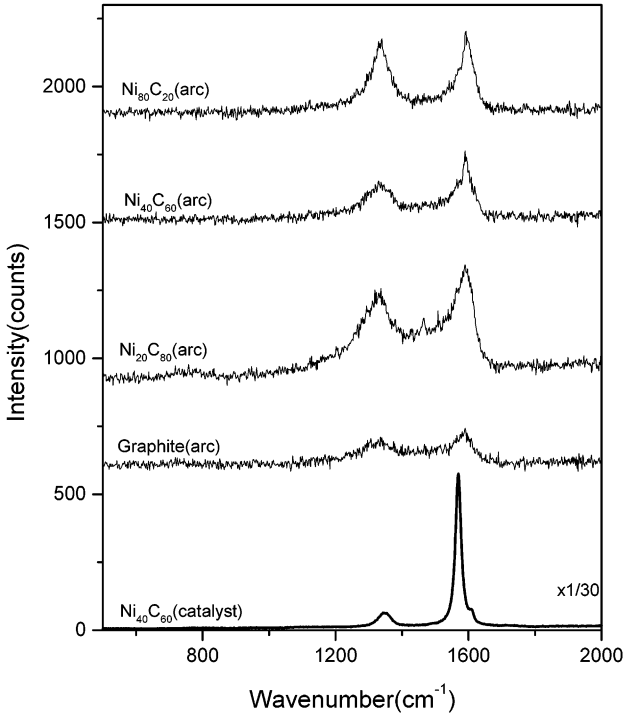

Figure 3. Raman shifts for the Ni-containing catalyst mixture and the arc-discharge deposits on the wall of the chamber. The arc-discharge derived products are denoted with the composition of their catalysts.

2 displays the XRD patterns for the Ni/C composites with various Ni contents. The XRD patterns of pure Ni and Ni/graphite mixture (the catalyst) are also included for comparison. The Ni peaks of the Ni/C composites become broad after the arc-discharge, in particular with lower Ni contents (<40 wt % Ni), implying a decrease in particle size. With increasing Ni content the Ni peaks become stronger and sharper, suggesting more and more big particles appear in the samples.

Raman spectra for the Ni−C samples are shown in Figure 3. For the mechanically mixed Ni(40 wt %) and graphite (see bottom line) two sharp carbon lines centered at ca. 1350 and

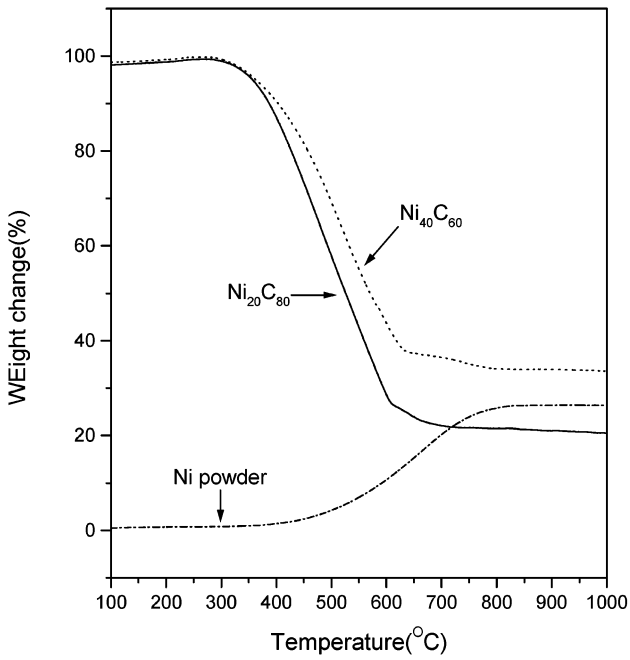

Figure 4. Metal content in Ni-containing samples measured by TPO method.

1577 cm^{-1} are observable. The band at 1350 cm^{-1} which is disorder-induced and usually called the D line is rather weak, whereas the 1577 cm^{-1} peak known as the G line[19,20] is very sharp and strong. After arc discharge, a striking increase in the relative intensity for D line is observable. The D-to-G line intensity ratio directly reflects the degree of the disorder in these carbon materials. Clearly the disordering is because of the newly formed nanostructures. Similar Raman spectra were observed for Co/C composites too. In Figure 3 the existence of a shoulder peak near 1570 cm^{-1} in the arc-charged Ni/C samples is noted. It could probably be ascribed to the A_{1g} radial breathing mode of single-walled carbon nanotubes (SWNTs), which were detectable by TEM in the samples.[21,22]

2. Temperature-Programmed Oxidation (TPO) Analysis of Metal Content in the Ni/C. Figure 4 displays the TPO results for graphite, Ni, $Ni_{20}C_{80}$ and $Ni_{40}C_{60}$, respectively, as measured by TGA in 10% O_2/Ar. It is seen that pure graphite could be burned out in O_2 at 600−900 °C, with only 0.50 wt % residual left. For pure Ni powder there is a weight increase of 26.3%, corresponding to the oxidation of metallic Ni to NiO. This value is slightly lower than the theoretical 28.3%, which may be attributed to the partial oxidation of the Ni powder, which has long been exposed to air. After burning in O_2 up to 1000 °C, 21 wt % and 33 wt % residuals are measured for $Ni_{20}C_{80}$ and $Ni_{40}C_{60}$, respectively, corresponding to 16.5 wt % Ni in $Ni_{20}C_{80}$-(arc) and 26.8 wt % Ni in $Ni_{40}C_{60}$(arc). It is interesting to note that the oxidation of carbon is much easier (at 300 degree lower) for carbon with metal addition than for pure graphite.

3. H_2 Chemisorption on Ni/C Composites. H_2 chemisorption on our Ni/C composites was studied by TPD, which has revealed that arc-discharge processing can increase H_2 uptake capacity of carbon. Figure 5 displays the hydrogen TPD profiles, obtained under conditions identical to those described in the Experimental Section, for the same amount of various Ni/C composites, which were pretreated with hydrogen under 35 atm from room temperature to 500 °C. Obviously the larger the peak area, the more hydrogen is desorbed, i.e., the more hydrogen has been stored in the samples before desorption. At the bottom of Figure

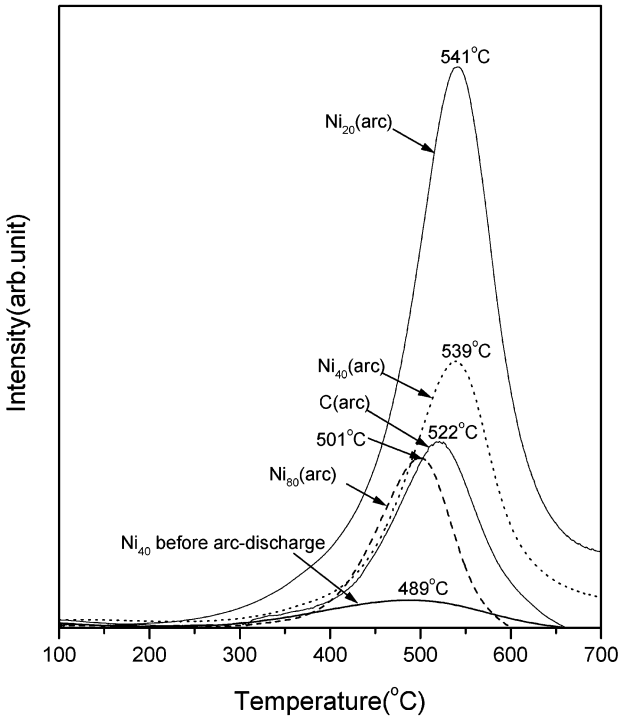

Figure 5. Hydrogen temperature-programmed-desorption profiles for various Ni/C composites. The adsorption of hydrogen was previously performed under 35 atm.

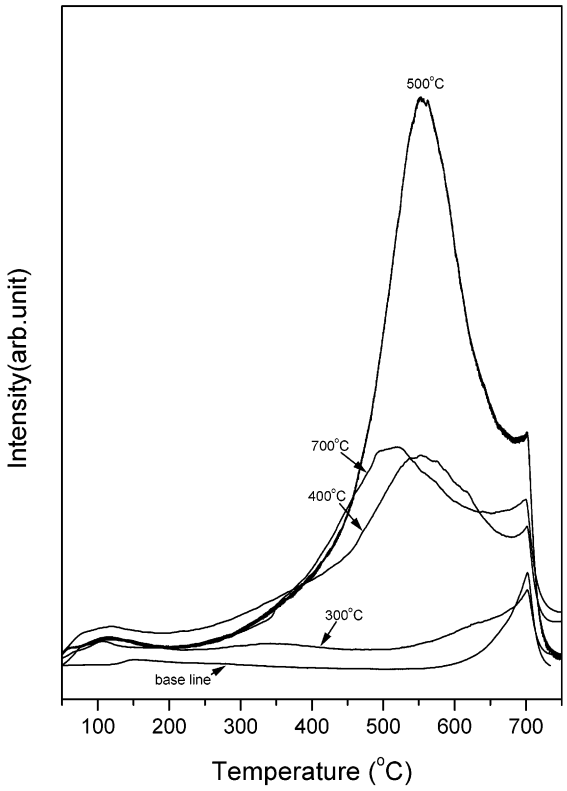

Figure 6. Hydrogen uptake of Ni_{20}(arc) at various adsorption temperatures under 35 atm.

5 an almost plain line is seen for the mechanically mixed Ni (40 wt %) and graphite (60 wt %) powders, indicating very poor hydrogen-storage capability of both nickel and graphite without arc-discharge processing. A similar result was also obtained from pure graphite or pure Ni powder as the test samples. However, a desorption peak centered at 522 °C is observed for the sample derived from pure graphite arc-discharge (Figure 5 C(arc)).

The addition of nickel in the anode catalyst has further enhanced the hydrogen-storage capability. A large desorption peak (corresponding to ca. 2.3 wt % H_2) centered at 541 °C is seen for the sample Ni_{20}(arc) which was prepared from arc-discharge with the catalyst containing 20 wt % Ni. Further increase of Ni content leads to a decrease in the hydrogen storage and a shift of peak maximum to lower temperatures. When the Ni content in the catalyst is reduced to 40 wt %, the peak (Ni_{40} arc) centered at 539 °C has its intensity about half that of Ni_{20}(arc). Nevertheless it is still higher than the arc-discharged graphite. When the Ni content is markedly increased up to 80 wt %, the peak shifts to 501 °C with a further decrease in intensity, which is even lower than that of the arc-discharged graphite. The decrease of hydrogen-storage capacity in the samples with high Ni content may result from the larger particle size of Ni in these samples. In a comparative experiment, the metal Ni in the arc-discharged sample, e.g., Ni_{20}(arc), was removed through a treatment with hydrochloric acid. The residual carbon exhibited a hydrogen uptake capacity very similar to that of arc-charged graphite, confirming that the increased hydrogen storage indeed partly comes from the metal addition. Though the adsorption/desorption of H_2 on these Ni/C composites both require high temperature (500 °C) and the storage capacity is not very high, the above results indeed show a promising way to increase the hydrogen storage of carbon materials by adding a suitable amount of highly dispersed transition metal.

The hydrogen uptake of the samples is strongly dependent on the adsorption temperature. TPD profiles in Figure 6 were obtained from Ni_{20}(arc) samples which were pretreated with hydrogen under 35 atm from room temperature up to different upper temperatures as labeled in the figure. It is seen that only a little amount of hydrogen can be stored in the sample pretreated in H_2 at 300 °C. When the upper pretreatment temperature was increased to 500 °C, a drastic enhancement of hydrogen uptake is found with 500 °C as the optimum temperature. As shown in the figure, the hydrogen uptake decreases for the 700 °C profile. A reasonable explanation is that a temperature lower than 500 °C may lead to an insufficient activation of H_2 molecules for some active sites while higher than 500 °C may result in the desorption of hydrogen from some adsorption sites.

Our experiments confirmed that when the hydrogen pressure was increased to 50atm, the hydrogen storage capacity would be increased to ca. 2.8 wt %. Adversely, under ambient pressure, almost no adsorbed hydrogen was detected in our above samples.

Samples collected from different places of the arc-discharge chamber showed different H_2 uptake capability. The hydrogen storage capacity of the deposits on the cathode in the arc-discharge chamber is about 30−40% of those deposits on the chamber wall. As revealed by the above TEM study the samples from different locations of the chamber may have different particle size and nano-structure, hence different H_2 storage capacity.

The above H_2 uptake−release process could be repeated many times (Figure 7). After the first 3 cycles, the hydrogen-storage capacity is decreased from initial 2.3 wt % to 1.8 wt %. Further increase of the cycles only leads to a slight decrease in the storage capacity. After 10 cycles, the hydrogen storage capacity remained at ca. 1.6 wt %.

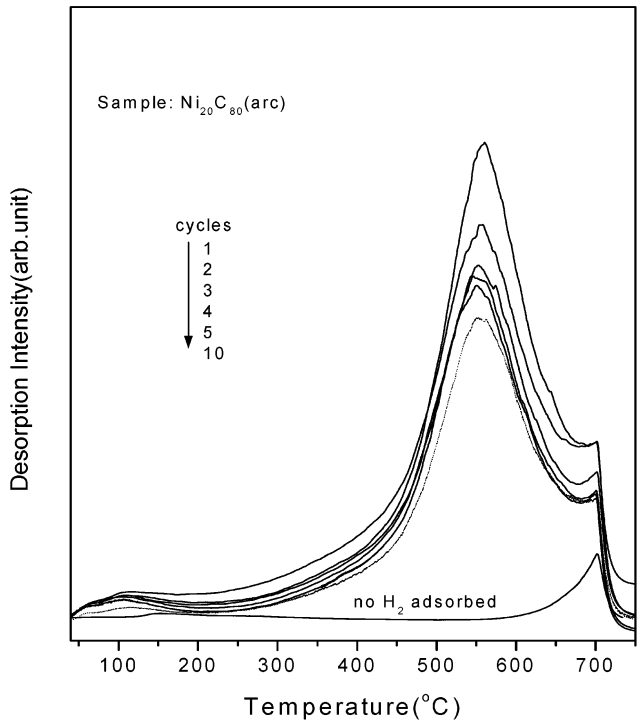

Figure 7. TPD profiles for Ni_{20}(arc) subjected to H_2 charge/discharge cycles. The bottom line is for the sample without prior hydrogen uptake.

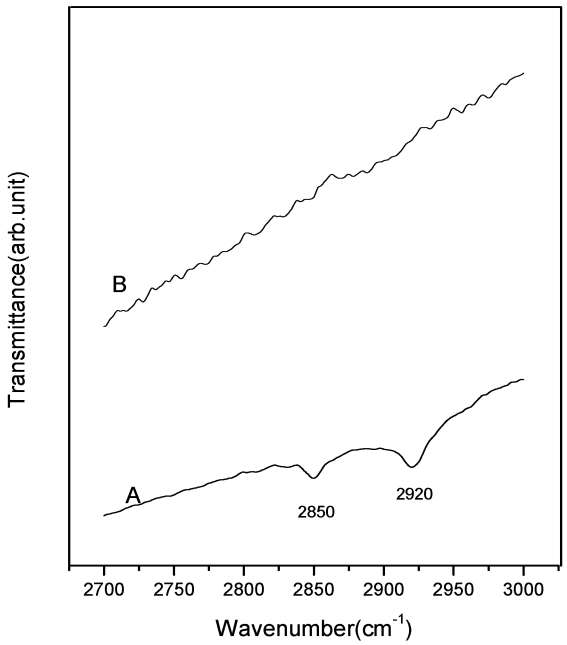

Figure 8. Infrared spectra for (a) Ni_{20}(arc), which was saturated with H_2 under 35 atm from room temperature to 500 °C and (b) Ni_{20}(arc), which was not exposed to H_2.

For cobalt-containing samples, a similar phenomenon was observed but with a higher desorption temperature (600 °C) and lower hydrogen storage capability (ca. 1.6 wt % for H_2 adsorption at 500 °C and 35 atm).

As shown in Figure 5 the arc-discharged graphite itself exhibits good hydrogen storage property, too, and high Ni contents (>40 wt %) may reduce the amount of hydrogen uptake. Therefore we believe that most of the hydrogen species should be adsorbed on carbon, not on Ni (or Co) while Ni (or Co) serves mainly as an active center to assist the dissociative adsorption of hydrogen molecules. This is evidenced in our in-situ FTIR studies. In Figure 8a, two weak feature bands at 2860 and 2920 cm^{-1} are discernible for an arc-discharged Ni/C sample, which was saturated with H_2 at 35 atm and 20−500 °C. These two bands are known to be due to the absorption arising from C−H stretching (symmetric and asymmetric, respectively) in sp^3 CH_2 species.[23,24] The samples without prior hydrogen adsorption and those without the addition of Ni do not exhibit the above C−H vibration bands (see Figure 8b). Their existence therefore indicates the existence of C−H bonds in this sample arising from H_2 chemisorption. It appears that hydrogen molecules are activated and dissociated at Ni sites. The H atoms would then spill onto nearby carbon sites, which are suitable for bonding/holding the hydrogen atoms. These two IR bands disappeared after heating the sample in an argon steam at elevated temperatures (>400 °C).

It is reported that nanosized metals or their alloys exhibit an improved kinetics of sorption and desorption for hydrogen compared to their counterparts with larger particle sizes.[25−27] A proposed explanation is that these nanosized structures possess a large number of grain boundaries and structural defects, which can provide bonding-unsaturated sites and easy paths for hydrogen adsorption and diffusion.[28] In our case, an arc-discharge method provides us a very useful and simple approach for preparing the nanocomposites containing carbon and nickel (or cobalt). The increased boundary structures should be responsible for the improvement of hydrogen storage in these materials. Our BET measurement of Ni/C composites has shown a drastic increase in specific surface area from 8.5 m^2/g for the mechanical mixture (20 wt % Ni and 80% graphite), to 130 m^2/g for Ni_{20}(arc). This change in specific surface area should be accompanied by a drastic increase in boundary structural sites in the sample, which, as discussed above, should be responsible for the enhancement of hydrogen storage capacity for the arc-discharged sample.

Interestingly it is noted that after H_2 charge/discharge cycles the Ni_{20}(arc) sample possesses larger specific surface area of 284m^2/g, while the carbon and nickel XRD peaks (the pattern not shown here) both become sharper. BET pore volume distribution measurement showed (see Figure 9) an increase in both pore volume (Figure 9a) and pore area (Figure 9b) after each cycle. So the increase in specific surface area of the sample should mainly come from the contribution of the newly formed pore structure. TEM image (Figure 1f) for this sample shows that some nickel particles in this sample have migrated out from the carbon matrix for the H_2 charge/discharge cycles, and even a few nickel particles have grown up to ca. 200 nm in diameter. The migration of Ni particles out from the carbon matrix is further evidenced by XPS study. Figure 10 compares the Ni $2p_{3/2}$ spectra for the Ni_{20}(arc) sample before and after H_2 uptake/release cycles. The peak is too weak to detect before H_2 adsorption (Figure 10a) but becomes observable after 5 cycles (Figure 10b), indicating the Ni particles have migrated out from the carbon encapsulation and segregated on the sample surface. The poorer dispersion of Ni appears to be the reason for the drop of the H_2 uptake capability after the first a few charge/discharge cycles, indicating the importance of the synergism between the transition metal active center and the hydrogen host carbon matrix.

4. H_2 Physisorption on Ni/C Composite. H_2 physisorption on the Ni/C composites were also measured by intelligent gravimetric analyzer (IGA) and pressure−composition isotherm (PCI), respectively. Figure 11a is a TG profile for the H_2 adsorption on arc-discharged Ni_{20}−C_{80} sample at 6 atm and cold temperatures. The adsorption starts at ca. −120 °C and reaches 0.6 wt % H_2 uptake at ca. −190 °C. The physical adsorption

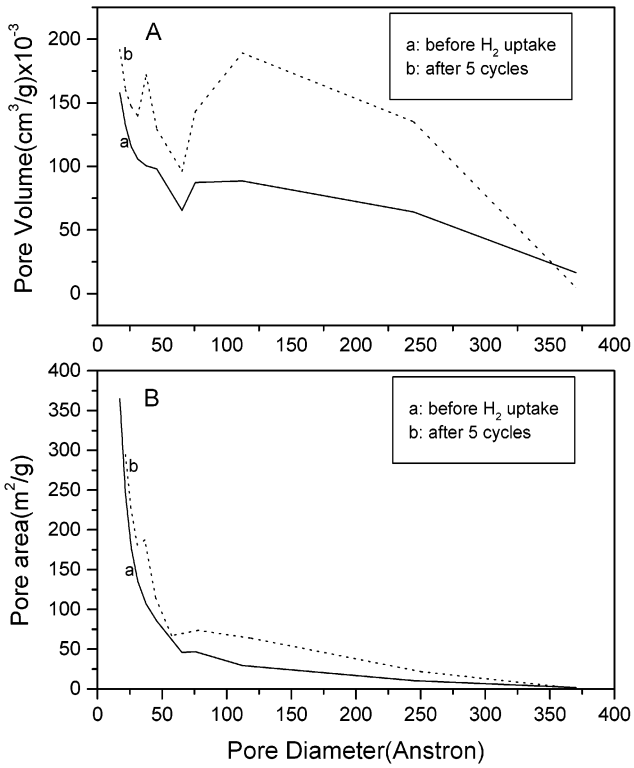

Figure 9. Pore volume distribution for Ni_{20}(arc) before hydrogen uptake (solid line) and after 5 cycles of hydrogen adsorption and desorption (dotted line).

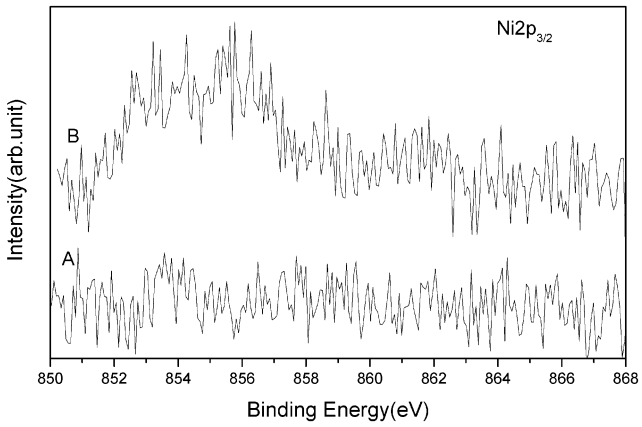

Figure 10. XPS $Ni2p_{3/2}$ spectra for Ni_{20}(arc) samples (a) before and (b) after 5 cycles of hydrogen uptake and desorption.

and desorption of hydrogen can be reversibly recycled many times. The small weight increase (<0.2 wt %) at temperatures between 0 and −120 °C is most probably due to the trace of moisture in the H_2 gas, the H_2 uptake by the sample under these conditions (−200 °C and 6 atm) is estimated to be 0.4 wt % only. At liquid nitrogen temperature the H_2 uptake was found to increase almost linearly with the increase of pressure. As measured by PIC, the hydrogen uptake is ca. 1.6 wt % at 35 atm and 2.7 wt % at 70 atm (Figure 11b).

In summary, we have demonstrated in this study that nanosized composites of carbon and nickel (or cobalt), in which Ni (or Co) is well dispersed in the nanosized carbon matrix, can be easily prepared by the arc-discharge method. The presence of suitable amount of Ni (or Co) can largely enhance the H_2 storage capacity of the Ni (or Co)/C composites. Up to 2.8 wt % H_2 has been measured at 500 °C and 50 atm on arc-discharged $Ni_{20}C_{80}$ using quantitative TPD. In-situ FTIR study

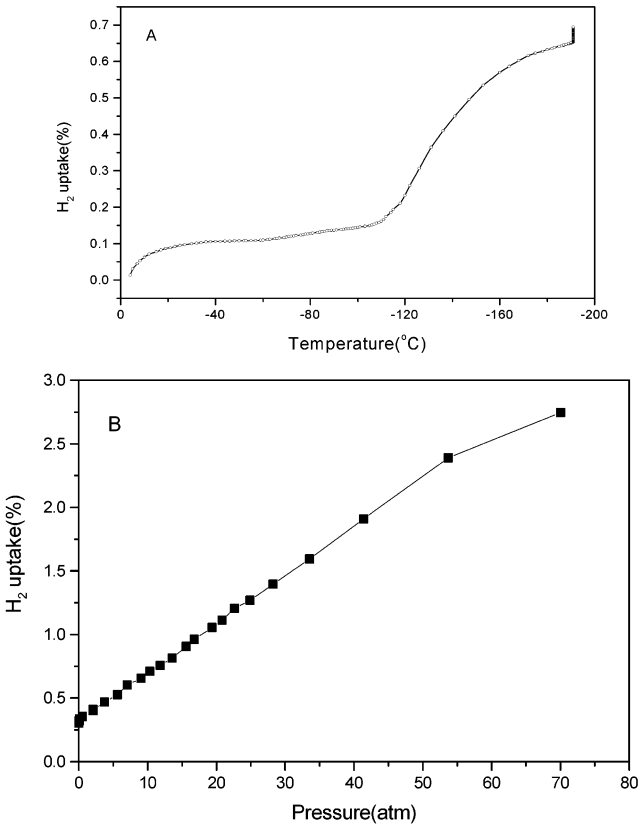

Figure 11. (A)The thermal gravimetric(TG) profile as measured by an IGA system for H_2 on the Ni_{20}(arc) sample at −200 °C to 0 °C and 6 atm; (B) H_2 physisorption capacity measured by PCI for the Ni_{20}-(arc) sample at liquid nitrogen temperature.

showed that at high temperatures hydrogen was dissociatively adsorbed and bonded to carbon. The high-temperature H_2 uptake and release could be repeated for many cycles, with a slight decrease in the H_2 storage capacity. Poorer dispersion of Ni in C after the cycles was found to be the main reason for the drop in the H_2 storage capability. At liquid nitrogen temperature and 70 atm the same sample can uptake 2.7 wt % H_2.

Acknowledgment. This work is supported by National Science and Technology Board of Singapore under the Research Grant GR6773. The authors thank Ms. Yanjiao Liu for XPS measurements.

References and Notes

(1) *Hydrogen in Metals* II; Alefeld, G., Vlkl, J., Eds.; Springer-Verlag: Berlin, Heidelberg, New York, 1978.
(2) Sastri, M. V. C. *Metals—Fundamentals and Applications*; Sastri, M. V. C., Viswanathan, B., Srinivasa Murthy, S., Eds.; Springer-Verlag Narosa Publishing House: Berlin, 1998; p 22.
(3) Orimo, S.; Fujii, H. *Appl. Phys. A* **2001**, *72*, 167.
(4) Ovshinsky, S. R.; Fetcenko, M. A. *Appl. Phys. A* **2001**, *72*, 245.
(5) Schlapbach, L.; Züttel, A. *Nature* **2001**, *414* (15), 353.
(6) Dillion, A. C.; Jones, K. M.; Bekkedahl, T. A.; Kiang, C. H.; Bethune, D. S.; Heben, M. J. *Nature* **1997**, *386*, 377.
(7) Chen, H. M.; Yang, Q. H.; Liu, C. *Carbon* **2001**, *39*, 1447.
(8) Liu, C.; Fan, Y. Y.; Liu, M.; Cong, H. T.; Cheng, H. H.; Dresselhaus, M. S. *Science* **1999**, *286*, 110.
(9) Dresselhaus, M. S.; Williams, K. A.; Eklund, P. C. *MRS Bull*. **1999**, *24*, 25.
(10) Zandonella, C. *Nature* **2001**, *410*, 734.
(11) Cao, A.; Zhu, H.; Zhang, X.; Li, X.; Ruan, D.; Xu, C.; Wei, B.; Liang, J.; Wu, D. *Chem. Phys. Lett.* **2001**, *342*, 510.
(12) Tibetts, G. G.; Meisner, G. P.; Olk, C. H. *Carbon* **2001**, *39*, 2291.
(13) Chen, P.; Wu, X.; Lin, J.; Tan, K. L. *Science* **1999**, *285*, 91.

(14) Yang, R. T. *Carbon* **2000**, *38*, 623.

(15) Pinkerton, F. E.; Wicke, B. G.; Olk, C. H.; Tibbetts, G. G.; Meisner, G. P.; Meyer, M. S.; Herbst, J. F. *J. Phys. Chem. B* **2000**, *104*, 9460.

(16) Schwarz, J. A. U.S. Patent 4,716,736, 1988.

(17) Ozaki, J.; Ohizumi, W.; Oya, A.; Illan-Gomez, M. J.; Roman-Martinez, M. C.; Linares-Solano, A. *Carbon* **2000**, *38*, 775.

(18) Imamura, H.; Takesua, Y.; Tabata, S.; Shigetomi, N.; Sakata, Y.; Tsuchiya, S. *Chem. Commun.* **1999**, 2277.

(19) Kastner, J.; Pichler, T.; Kazmany, H.; Curran, S.; Blau, W.; Weldon, D. N.; Delamesiere, M.; Draper, S.; Zandbergen, H. *Chem. Phys. Lett*. **1994**, *221*, 53.

(20) Tang, P. H.; Zhang, S. L.; Yue, K. T.; Huang, F. M.; Shi, Z. J.; Zhou, X. H.; Gu, Z. N. *J. Raman Spectosc.* **1997**, *28*, 369.

(21) Bacsa, R. R.; Laurent, C.; Peigney, A.; Basca, W. S.; Vaugien, T.; Rousset, A. *Chem. Phys. Lett*. **2000**, *323*, 566.

(22) Tang, S.; Zhong, Z. Y.; Xiong, Z.; Sun, L.; Liu, L.; Jin, J.; Tan, K. L. *Chem. Phys. Lett.* **2001**, *350*, 19.

(23) Nakamoto, K. *Infrared and Raman Spectra of Inorganic and Coordination Compounds*, 4th ed.; John Wiley & Sons, Inc.: New York, 1986.

(24) Xu, J.; Huang, X.; Li, W.; Li, W.; Huang, X.; Chen, K.; Xu, J.; Wilson, I. H. *Appl. Phys. Lett.* **2001**, *79*, 141.

(25) Zasuski, L.; Hosatte, S.; Tssier, P.; Ryan, D. H.; Ström-Olsen, J. O.; Trudeau, M. L.; Svchulz, R. *Metal−hydrogen systems*; M. R. Oldenbourg Verlag: Uppsala, 1992; p. 1067.

(26) Zaluski, A.; Zaluski, A.; Ström-Olsen, J. O. *J. Alloys Compd.* **1999**, *290*, 71.

(27) Zaluski, A.; Zaluski, A.; Ström-Olsen, J. O. *J. Alloys Compd.* **2000**, *298*, 125.

(28) Zaluski, A.; Zaluski, A.; Ström-Olsen, J. O. *Appl. Phys*. **2001**, *72*, 157.